Journal of Thermal Analysis and Calorimetry, 94 (2008) 2, 379–387

THERMAL BEHAVIORS OF AMORPHOUS CALCIUM CARBONATES PREPARED IN AQUEOUS AND ETHANOL MEDIA

N. Koga and Y. Yamane*

Chemistry Laboratory, Graduate School of Education, Hiroshima University, 1-1-1 Kagamiyama, Higashi-Hiroshima 739-8524, Japan

Two different samples of amorphous calcium carbonate (ACC) hydrates were prepared respectively by mixing aqueous solutions of $CaCl_2$ and Na_2CO_3–NaOH and by allowing the diffusion of $(NH_4)_2CO_3$ sublimate into ethanol solution of $CaCl_2$. Thermal behaviors of the synthetic ACCs were investigated comparatively by means of thermoanalytical techniques complimented by powder X-ray diffraction, FTIR spectrometry and microscopic observations. The anhydrous ACCs produced by the thermal dehydration of the respective samples were crystallized to calcite in different ways. The sample prepared in aqueous medium was crystallized at around 600 K in a single step. Crystallization in two separated steps at around 600 and 825 K was observed for the sample prepared in ethanol medium. Characteristics of the crystallization processes were discussed from thermodynamic and kinetic points of view.

Keywords: *amorphous calcium carbonate, crystallization, kinetics, thermal behavior*

Introduction

In addition to three well-known crystalline polymorphs of calcite, aragonite and vaterite, calcium carbonate exists as metastable amorphous phases of hydrate and anhydrate [1–4]. The amorphous calcium carbonates (ACC) are found in many animals and plants as a transient phase of biomineralization of crystalline $CaCO_3$ [5–9] and also as a possible storage form of calcium ion [10]. The roles of ACC to transform a selected crystalline polymorph of $CaCO_3$ with a specialized morphology and/or architecture in living organisms are special interest, as well as the mechanisms of stabilization of intrinsically metastable ACC. Learning from biomineralization of $CaCO_3$ in living organisms [5–12], ACCs are attracting attentions recently in the differently oriented material researches, i.e., nano-sized functional materials [13–17], inorganic–organic hybrid materials [18–20], thin films [21–26] and so on. In all the cases, sophisticated kinetic controls of the nucleation and growth processes of the desired crystalline phase by preventing nucleation of undesired phase in a matrix of ACC are one of the key to promoting those researches [27–34].

Although various preparation methods of ACC with or without additives are known, transformation properties and/or stability of the synthetic ACC change depending on the preparation methods and also on the reaction conditions in the respective preparation methods. This seems to be due to varieties of synthetic ACC in views of thermodynamic state, characterized by degree of atomic disordering and particle aggregation, and crystallization kinetics, characterized by probability of possible nucleation sites and atomic diffusion for crystal growth [7, 35, 36]. For example, when preparing ACC by one of the simplest methods of mixing a $CaCl_2$ solution with a Na_2CO_3–NaOH solution [37], the enthalpy changes due to thermally induced crystallization of dehydrated ACC to calcite change largely from –4.0 to –12.3 kJ (mol $CaCO_3$)$^{-1}$ with the slight change of the pH values of the mother solution from 12.2 to 13.0 [35]. Accompanying with such change of thermodynamic state of dehydrated ACC with the preparation condition, the apparent activation energy for the crystallization process increases from 152 to 304 kJ mol^{-1}. Accordingly, evaluation and control of specific characteristics of ACC are essentially important in the variously orientated studies using ACC as a raw material, where thermoanalytical techniques can be one of the most powerful tools for characterizing ACC from the view points of thermal stability based on thermodynamics and crystallization kinetics.

In the present study, we focused on ACC precipitated in an ethanol solution of anhydrous $CaCl_2$ by the dissolutions of gaseous CO_2, NH_3 and H_2O originated from solid $(NH_4)_2CO_3$ placed next to the ethanol solution in a closed system. Unusual stability of the gel-like precipitate of ACC in the mother ethanol solution, which barely transforms to crystalline $CaCO_3$, has recently been reported by Lee *et al*. [38]. The thermal behavior of the as-prepared ACC in the ethanol medium was characterized by several thermoanalytical techniques, in comparison with the ACC prepared in an aqueous medium.

* Author for correspondence: nkoga@hiroshima-u.ac.jp

1388–6150/$20.00

Akadémiai Kiadó, Budapest, Hungary
Springer, Dordrecht, The Netherlands

Experimental

Sample preparation

Amorphous calcium carbonates termed as ACC-AQ and ACC-ET were prepared by two different methods in an aqueous and ethanol media according to the methods reported previously by Kojima *et al*. [37] and Lee *et al*. [38], respectively. For the fabrication of ACC-AQ, every 100 cm^3 of aqueous solutions of sodium carbonate (0.1 mol dm^{-3}) and sodium hydroxide (0.1 mol dm^{-3}) were mixed with mechanical stirring to obtaining a stock solution of pH≈13. The stock solution was stored in a refrigerator at 273 K for more than 1 h, together with an alternative stock solution of 100 cm^3 of calcium chloride (0.1 mol dm^{-3}). Using a cooling stirrer (CSB-900N), two stock solutions were mixed rapidly in a beaker (500 cm^3) at an ambient temperature of 273 K. The precipitated colloidal phase was filtered immediately and washed with ice–water. The precipitate was dried in a vacuum desiccator for one day and stored in a refrigerator at 263 K.

According to Lee *et al*. [38], ACC-ET was prepared from an ethanol solution of anhydrous calcium chloride ($1.0 \cdot 10^{-2}$ mol dm^{-3}) and solid ammonium carbonate, where a regent grade of ethanol (≥99.5%: Sigma Aldrich Japan) was utilized. Ammonium carbonate (10 g) was spread in a cylindrical separable flask (500 cm^3). A beaker (200 cm^3) with 200 cm^3 of ethanol solution of anhydrous calcium chloride ($1.0 \cdot 10^{-2}$ mol dm^{-3}) was placed in the separable flask. Using a lid for the separable flask, the reaction vessel was sealed up. The closed reaction vessel was left at a controlled ambient temperature of 293 K for 24 h. A milky-white colloidal phase as precipitated was filtered and washed with ethanol. The precipitate was dried in a vacuum desiccator for 4 h and stored in a refrigerator at 263 K.

Measurements

Powder X-ray diffraction (XRD) patterns of the samples, ACC-AQ and ACC-ET, were recorded using an instrument of Rigaku RINT2200V (monochrome CuK_α, 40 kV, 20 mA). Fourier transformation infrared (FTIR) spectra were measured, using an instrument of Shimadzu FTIR8400S, by the diffuse reflectance method after diluting the samples with KBr. TG-DTA measurements were carried out using a ULVAC TGD9800 where the samples of 10.0 mg were heated linearly at a heating rate of 10 K min^{-1} under flowing N_2 at a rate of 100 cm^3 min^{-1}. Morphologies of the samples were observed using a scanning electron microscope (Hitachi S-2460N).

About 5 mg of samples weighed onto a platinum cell (5 mmϕ and 2.5 mm in height) were subjected to the measurements of TG/DTA-MS. Using an instrument of TG/DTA-MS constructed by coupling a TG-DTA (Rigaku TG8120) with a quadrupole mass spectrometer (Anelva M-200QA), TG-DTA curves were recorded on heating at 10 K min^{-1} under flowing He (200 cm^3 min^{-1}), accompanied by continuous measurements of the mass spectra of the evolved gases (mass range: 10–50 amu, EMSN: 1.0 A, SEM: 1000 V). Phase changes during heating the samples from room temperature to 1100 K were followed using the above described XRD instrument by equipping with a programmable heating chamber (Rigaku PTC-20A). By heating the samples at a linear heating rate of 5 K min^{-1} under flowing N_2 at 100 cm^3 min^{-1}, XRD patterns were measured at various temperatures where the sample temperature was kept constant during the diffraction measurements. For characterizing the crystallization behavior of amorphous calcium carbonate anhydrate appeared during the course of heating the samples, measurements of differential scanning calorimetry (DSC: Shimadzu DSC60) were carried out at different heating rates from 2 to 10 K min^{-1} under flowing N_2 (50 cm^3 min^{-1}), where the samples of 5.0 mg were weighed onto a platinum cell (5 mm in diameter and 2.5 mm in height) and covered with a platinum lid. For covering the temperature range higher than 800 K, high temperature DSC (Rigaku DSC8270) was also applied under the measuring conditions identical with the above DSC runs.

Results and discussion

Characterization of samples

Figure 1 compares typical SEM images of the samples, ACC-AQ and ACC-ET, prepared in aqueous and ethanol media, respectively. Although both the samples appear as aggregates of nano-sized particles, it is apparent that ACC-ET represents the more homogeneous gel-like aggregates. Figure 2 shows the powder XRD patterns of the samples. Although both the samples indicate no distinguished XRD peak, the centers of halos are observed at different diffraction angles, i.e., around 32 and 27.5 for ACC-AQ and ACC-ET, respectively. FTIR spectra of the samples are shown in Fig. 3. No distinguished difference can be seen for the FTIR spectra of the samples. It is also noted that these spectra are very similar to those for the biogenic ACC [7, 10, 12]. Broad absorption bands around 3400–3500 and 1400–1500 cm^{-1} correspond to O–H stretching vibration of hydrated water and ν_3 mode of carbonate ion, respectively. The broadened and/or split absorption peaks of ν_3 mode of carbonate ions at 1400–1500 cm^{-1} indicate a lock of symmetry in the

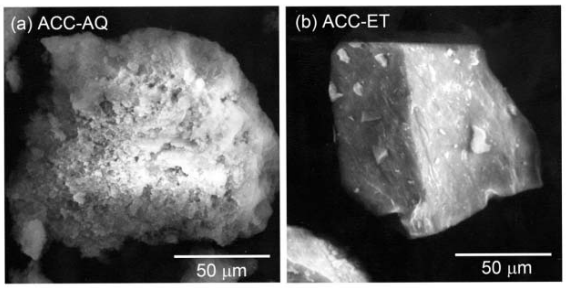

Fig. 1 Typical SEM images of a – ACC-AQ and b – ACC-ET

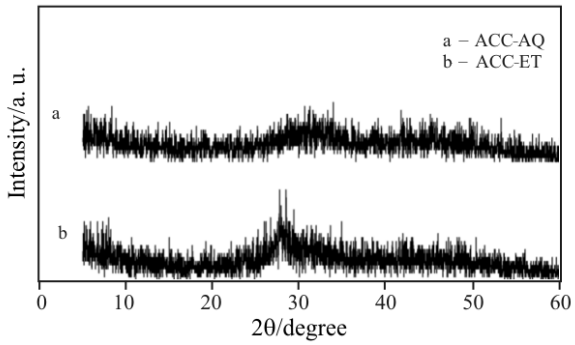

Fig. 2 Typical powder XRD patterns of ACC-AQ and ACC-ET

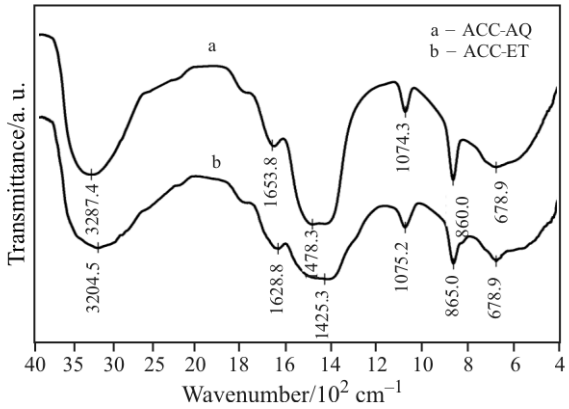

Fig. 3 Typical FTIR spectra of ACC-AQ and ACC-ET

carbonate ions [7]. Appearance of ν_1 mode of carbonate ions at around 1075 cm^{-1} is also due to non-centrosymmetric structure, which is also observed for crystalline aragonite and vaterite [28, 39, 40].

Thermal behaviors

Figure 4 represents typical TG-DTA curves of the samples. For both the samples, mass losses initiate near room temperature just after starting heating program. During heating the samples up to 600 K, total mass losses of 20.0±0.4 and 22.0±0.7%, which seem to be due to dehydration of hydrated water, are observed for ACC-AQ and ACC-ET, respectively. From the shapes of TG-DTA curves, the dehydration process proceeds via two separated mass loss steps, where well separated two step dehydration is observed more clearly for ACC-ET. Figure 5 shows typical mass-chromatograms of *m*/*z* 18 and 44 recorded for the evolved gases during the dehydration process under flowing He (200 cm^3 min^{-1}). It is seen that small amount of CO_2 is evolved during this reaction stage together with H_2O, which seems to be due to CO_2 and/or HCO_3^- trapped in the gel precipitate [37, 41, 42]. As was expected from the shapes of TG-DTA curves, evolutions of H_2O and/or CO_2 take place in some more clearly separated two steps in ACC-ET. The two separated dehydration behavior is also reported for the biogenic ACC [8, 10].

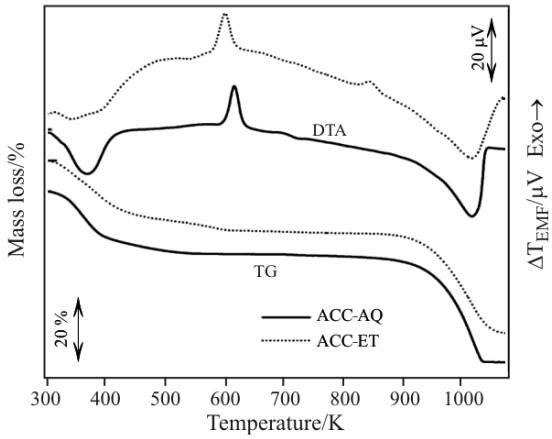

Fig. 4 Typical TG-DTA curves for ACC-AQ and ACC-ET recorded at a heating rate of 10 K min^{-1} in flowing N_2

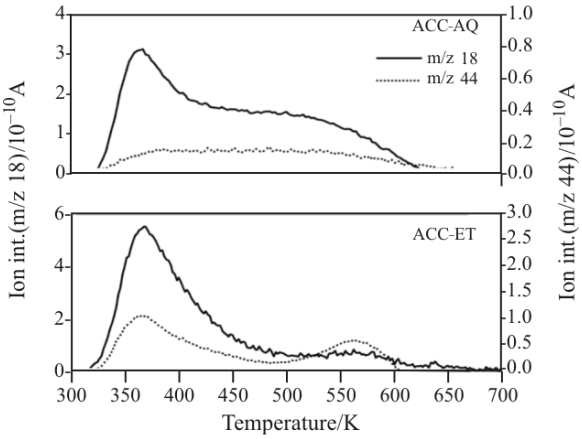

Fig. 5 Typical mass-chromatograms of *m*/*z* 18 and 44 for the evolved gases during the thermal dehydration of ACC-AQ and ACC-ET

Just after the dehydration processes were completed, an exothermic peak is observed for both the samples, Fig. 4. Under a linearly increasing temperature at 10 K min^{-1}, extrapolated onset temperature of the exothermic peak of ACC-AQ is higher by 15 K than that of ACC-ET. Figure 6 shows changes of the powder XRD patterns of the samples during stepwise

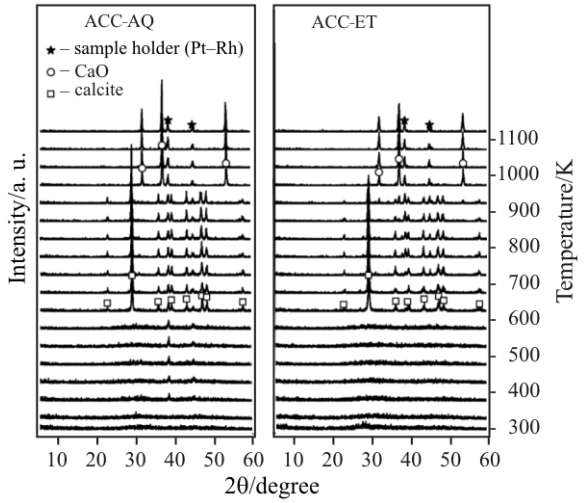

Fig. 6 Changes of powder XRD patterns on heating ACC-AQ and ACC-ET

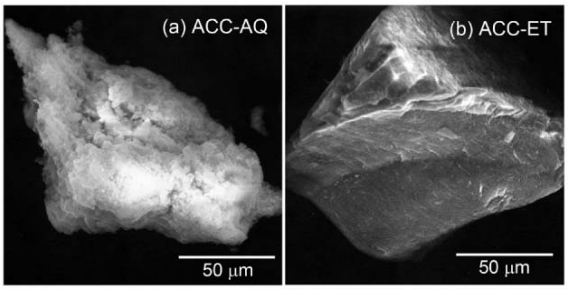

Fig. 7 Typical SEM images of a – ACC-AQ and b – ACC-ET heated to 643 K

heating at a heating rate 10 K min^{-1} and holding for 10 min for diffraction measurements at various temperatures. During the thermal dehydration process, no distinguished diffraction peak appears. At 623 K just after the DTA exothermic peak, diffraction pattern of calcite appears in both the samples as has been reported previously [35, 37]. Figure 7 shows typical SEM images of the samples heated to 643 K. As for ACC-AQ, a stacking structure constructed by sheet aggregates of crystallized particles is observed. Appearances of ACC-ET do not change largely by the crystallization, but a banded structure lined up a specific direction is observed on the selected surfaces of the gel-like aggregates. The above observations indicate that, for both ACC-AQ and ACC-ET, two dimensional development of crystallites network plays an important role in the crystallization of calcite from amorphous calcium carbonate. Details of XRD patterns and IR spectra of the crystallized samples are compared in Figs 8 and 9. In comparing the XRD patterns of the samples at 623 K shown in Figs 8a and b, while the single phase of calcite is confirmed in Fig. 8a for ACC-AQ, several diffraction peaks due to vaterite are observed in Fig. 8b for ACC-ET as a miner phase in

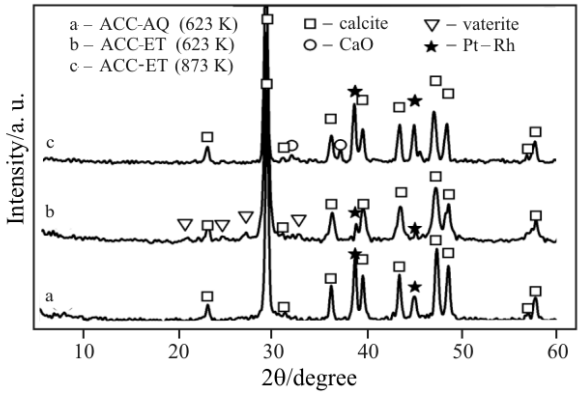

Fig. 8 Typical powder XRD patterns of ACC-AQ and ACC-ET heated to several selected temperatures

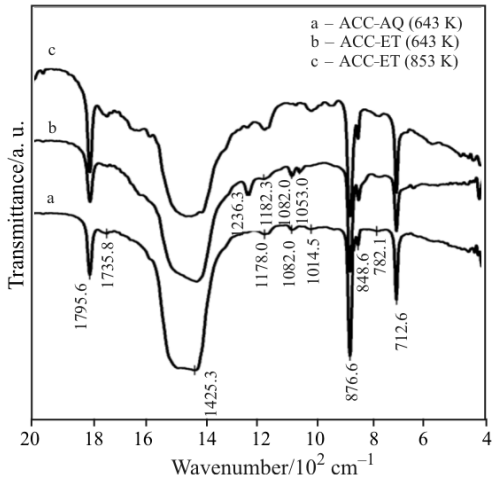

Fig. 9 Typical FTIR spectra of ACC-AQ and ACC-ET heated to several selected temperatures

the major phase of calcite. Deducing from the comparisons of intensities and half-width of the respective corresponding diffraction peaks of calcite, it is also expected that the growth of crystalline particles of calcite is more remarkable for ACC-AQ than ACC-ET. In the IR absorption spectra of the samples at 643 K just after calcite crystallization, shown in Figs 9a and b, all the major peaks due to IR vibration modes of CO_3^{2-} in calcite are observed, i.e., at 877 cm^{-1} (ν_2), ~1425 cm^{-1} (ν_3) and 713 cm^{-1} (ν_4) [39]. Differences can be seen for the weak absorption peaks appeared in the range of 1000–1250 cm^{-1}, where split peaks at 1055 and 1082 cm^{-1} observed in Fig. 9b for ACC-ET at 643 K, together with the peak at 1236 cm^{-1}, are likely due to the stretching vibrations of CO_3^{2-} in vaterite contaminated as the miner phase.

On further heating, the second exothermic peak is observed only for ACC-ET at around 800–850 K before decomposition of calcite, Fig. 4. The powder XRD pattern and IR spectrum of ACC-ET after the second exothermic peak are shown in Figs 8c and 9c, respectively. Both the powder XRD pattern and IR

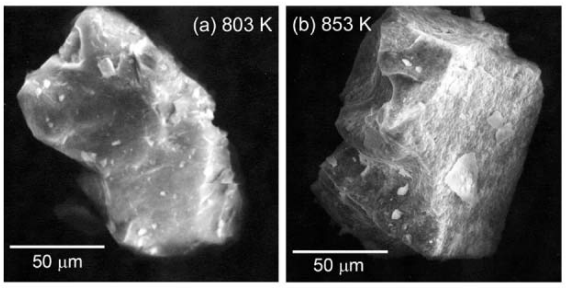

Fig. 10 Typical SEM images of ACC-ET at temperatures just a – before and b – after the second exothermic effect of crystallization

spectrum are clearly corresponding to those for calcite, except small XRD peaks due to CaO produced by the partial decomposition of calcite. Figure 10 compares typical SEM images of ACC-ET at 803 and 853 K which are just before and after the second exothermic peak, respectively. At 803 K before the second exothermic peak, the sample particle indicates the gel-like aggregate with smooth surface textures, by remaining the characteristic texture of original ACC-ET unchanged. Surface textures of ACC-ET change drastically during the second exothermic peak as is seen in Fig. 10b, where destruction of the original structure of gel-like aggregate and development of stacking layer of calcite phase are observed. The above findings concerning the physico-chemical events taking place during the second exothermic peak for ACC-ET indicate the crystal growth of calcite in the poorly crystalline phase that has been produced during the first exothermic peak of crystallization. The calcite crystallization separated in two steps seems to result from the rigid gel structure of ACC-ET, which disturbs the crystal growth of calcite during the first exothermic peak. The rightly stacking structure of calcite is constructed by the effect of such rigid gel structure characteristic for ACC-ET and through the crystallization in two separated steps.

The subsequent mass loss accompanying with extensive DTA endothermic peak initiates at around 850 K, indicating the mass losses of 42.6±1.1 and 42.6±1.0% on the basis of dehydrated samples for ACC-AQ and ACC-ET, respectively. The observed mass loss values are nearly corresponding to the theoretical value of 44.0% calculated by assuming the thermal decomposition:

$$CaCO_3 \rightarrow CaO + CO_2$$

Enthalpy changes and kinetics of thermally induced crystallization processes from dehydrated ACC to calcite

On the basis of DSC at different heating rates, the thermally induced crystallization processes of dehydrated ACC-AQ and ACC-ET were characterized from the view points of thermodynamics and kinetics. Figures 11 and 12 show the DSC traces for the first exothermic processes of ACC-AQ and ACC-ET, respectively. The areas of DSC peaks do not change depending on heating rate applied, indicating the averaged enthalpy changes ΔH of –13.1±0.2 and –19.1±0.2 kJ (mol $CaCO_3$)$^{-1}$ for ACC-AQ and ACC-ET, respectively. The value of ΔH determined in the present study for ACC-AQ is closely corresponding to that reported previously for the crystallization process of dehydrated ACC prepared by the identical method in aqueous medium, i.e., –12.3±0.2 kJ (mol $CaCO_3$)$^{-1}$ [35] and also to that reported by Wolf and Gunther, i.e., –15.0±3.0 kJ mol^{-1} [43]. Despite two step crystallization of amorphous $CaCO_3$ to calcite observed for ACC-ET, the value of ΔH for the first crystallization step, –19.1±0.2 kJ (mol $CaCO_3$)$^{-1}$, is larger than that for ACC-AQ which crystallizes in single step. This means that the state of amorphous $CaCO_3$ produced by the thermal dehydration of ACC-ET is unstable thermodynamically compared with that of ACC-AQ.

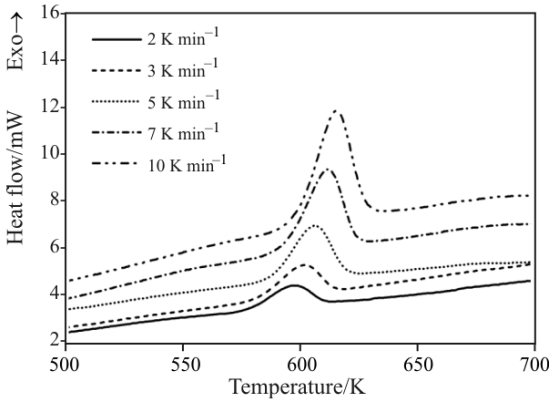

Fig. 11 Typical DSC curves for the crystallization of dehydrated ACC-AQ at various heating rates

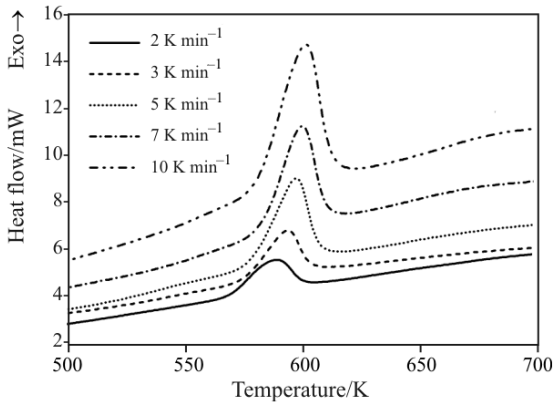

Fig. 12 Typical DSC curves for the first crystallization step of dehydrated ACC-ET at various heating rates

The series of DSC traces at different heating rates shown in Figs 11 and 12 were subjected to the kinetic analyses. Firstly, the apparent activation energies, E_a, at various fractional conversions, α, were determined by the Friedman method [44] using the relationship between the rate of conversion, dα/dt, and the absolute temperature, T.

$$\ln\frac{\mathrm{d}\alpha}{\mathrm{d}t} = -\frac{E_a}{RT} + \ln[Af(\alpha)] \quad (1)$$

where R, A and $f(\alpha)$ are the gas constant, Arrhenius pre-exponential factor and kinetic model function in a differential form. Within a selected range of $0.1 \le \alpha \le 0.9$, the plots of ln(dα/dt) *vs.* T^{-1} at various constant α indicated fairly linear correlations with the averaged correlation coefficients of –0.9975 and –0.9805 for ACC-AQ and ACC-ET, respectively. The values of E_a calculated from the slopes of the Friedman plots at various α for the crystallizations of dehydrated ACC-AQ and ACC-ET are compared in Fig. 13. Although a trend of increasing the value of E_a with α is observed for both the samples, the change is less than the standard deviation of 7% in the restricted range $0.1 \le \alpha \le 0.9$ indicating the averaged E_a values of 270.7±15.1 and 379.8±26.0 kJ mol^{-1} for ACC-AQ and ACC-ET, respectively. The E_a value of 270.7±15.1 kJ mol^{-1} evaluated for ACC-AQ is in good agreement with that reported previously for the crystallization of dehydrated ACC prepared by the identical method in aqueous medium, i.e., 304.1±23.6 kJ mol^{-1} [35]. The value of E_a estimated for ACC-ET is larger by over 100 kJ mol^{-1} than that for ACC-AQ, contrary to the exothermic peaks of crystallization being observed at the slightly lower temperatures.

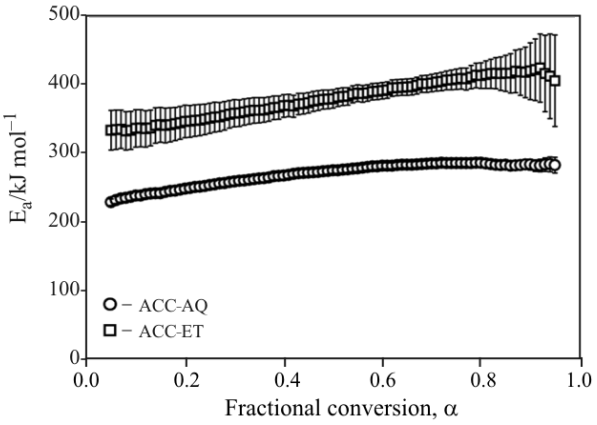

Fig. 13 The values of E_a at various α for the crystallization of dehydrated ACC-AQ and ACC-ET (1st step)

The isothermal rate behaviors of the crystallization were simulated by extrapolating the measured rate data to infinite temperature using the Ozawa's generalized time θ [45–47]:

$$\theta = \int_0^t \exp\left(-\frac{E_a}{RT}\right)\mathrm{d}t \quad (2)$$

The conversion rate at infinite temperature, dα/dθ, can be calculated using the isoconversional relationship of the Friedman plots at selected α according to the following equation [48, 49]:

$$\frac{\mathrm{d}\alpha}{\mathrm{d}\theta} = \frac{\mathrm{d}\alpha}{\mathrm{d}t}\exp\left(\frac{E_a}{RT}\right) \quad (3)$$

Figure 14 represents the plots of dα/dθ *vs.* α for the crystallizations of dehydrated ACC-AQ and ACC-ET, where error bars indicate the standard deviation of the dα/dθ values calculated from the respective experimental data at different heating rates. Large differences can be seen between the isothermal rate behaviors of the samples. The crystallization rate behavior of the dehydrated ACC-AQ is characterized by the peak maximum at α=0.25, indicating the consecutive and/or concurrent processes of nucleation and growth. On the other hand, a linearly decelerating process is estimated for the first crystallization step of the dehydrated ACC-ET.

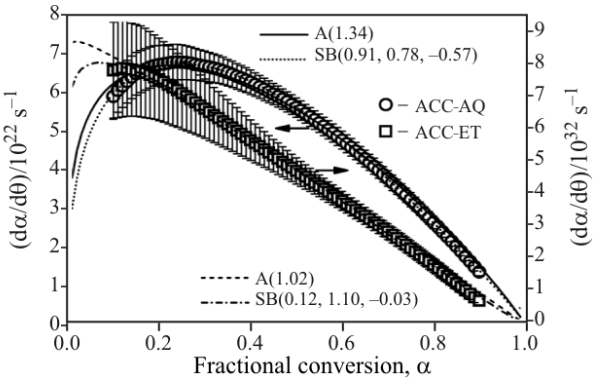

Fig. 14 Isothermal rate behaviors simulated at infinite temperature for the crystallization of dehydrated ACC-AQ and ACC-ET (1st step)

The isothermal kinetic data at infinite temperature expressed by a plot of dα/dθ *vs.* α can be related to the value of A and $f(\alpha)$ by the following equation [48, 49]:

$$\frac{\mathrm{d}\alpha}{\mathrm{d}\theta} = Af(\alpha) \quad (4)$$

In the present study, a physico-geometric $f(\alpha)$ of nucleation and growth type, A(m), i.e. Johnson–Mehl–Avrami–Erofeev–Kohlmogorov model [50–53], was employed by introducing the non-integral kinetic exponent m [54–58]. An empirical $f(\alpha)$ with three non-integral kinetic exponents SB(m, n, p), Šesták–Berggren model [59], was also applied for supporting the interpretations of the kinetic fitting by

Table 1 Summary of the kinetic results for the thermally induced crystallization of dehydrated ACC-AQ and ACC-ET in a restricted range $0.1 \leq \alpha \leq 0.9$

Sample	E_a/kJ mol^{-1}	$f(\alpha)$	A/s^{-1}
ACC-AQ	270.7±15.1	A(1.34) SB(0.91, 0.78, –0.57)	$(9.19\pm0.03)\cdot10^{22}$ $(1.48\pm0.02)\cdot10^{23}$
ACC-ET	379.8±26.0	A(1.02) SB(0.12, 1.10, –0.03)	$(9.40\pm0.03)\cdot10^{32}$ $(1.10\pm0.03)\cdot10^{33}$

A(m). The kinetic model functions, A(m) and SB(m, n, p), are expressed by the following equations, respectively.

$$A(m)=m(1-\alpha)[-\ln(1-\alpha)]^{1-1/m} \quad (5)$$

$$SB(m, n, p)=\alpha^m(1-\alpha)^n[-\ln(1-\alpha)]^p \quad (6)$$

By applying the Lovenberg–Marquardt optimization algorithm [60], the most appropriate values of kinetic exponents and the value of A were determined simultaneously by the nonlinear least square fitting based on Eq. (4) [61].

As shown in Fig. 14, the crystallization processes of the dehydrated ACC-AQ and ACC-ET were fairly good fitted by the nucleation and growth model A(m) with m=1.34 and m=1.02, respectively. Using the empirical model of SB(m, n, p), the isothermal rate data at infinite temperature are nearly perfectly fitted due to really empirical characteristic of the function to accommodate various physico-geometric types of reactions including those deviated cases [59, 61, 62]. The crystallization rate behavior of the dehydrated ACC-AQ was best fitted by SB(0.91, 0.78, –0.57). Although the physico-geometrical meanings of the kinetic exponents are not clear in this case, the fitting curve of SB(0.91, 0.78, –0.57) is in good agreement with that of A(1.34), indicating the validity of A(1.34) as the suitable $f(\alpha)$. The function A(m) with $m\approx1.5$ is interpreted physico-geometrically as the three-dimensional growth of pre-existing nuclei controlled by diffusion or as the constant rate nucleation and subsequent one-dimensional growth controlled by diffusion [50–53]. As for the first crystallization step of the dehydrated ACC-ET, the empirical SB(0.12, 1.10, –0.03) was selected as the best function. Because the function A(m) with m=1.0 corresponds to SB(0, 1.0, 0), the functions A(1.02) and SB(0.12, 1.10, –0.03) is taken as practically identical. Because the crystal growth of calcite is restrained by the rigid gel structure of the substrate in the first crystallization step of the dehydrated ACC-ET, the first order rate behavior expressed by the A(m) with $m\approx1.0$ seems to indicate the kinetic process controlled by the constant rate nucleation or two-dimensional growth of pre-existing nuclei controlled by diffusion [50–53].

The kinetic results for the crystallization of the dehydrated samples are summarized in Table 1. By considering the coefficient m in A(m) law, Eq. (5), the values of A evaluated assuming A(m) and SB(m, n, p) laws are practically identical within the respective samples. The values of A evaluated for the respective samples are largely different following with the distinguished difference in the E_a values. Although the crystallization processes of the respective samples are characterized by largely different sets of A and E_a due to the difference of the physico-geometric mechanism, the respective sets of A and E_a describe the processes taking place in a similar temperature region, which is explained by the kinetic compensation effect between the values of A and E_a [50–53, 63–66].

As described above, the second exothermic peak of crystallization is observed for ACC-ET at around 800–850 K just before the thermal decomposition of calcite. Figure 15 shows typical DSC curves for the second exothermic effect of ACC-ET. In contrary to the constant ΔH value, –19.1±0.2 kJ (mol $CaCO_3$)$^{-1}$, observed for the first exothermic effect irrespective of heating rate applied, the value of ΔH for the second exothermic effect varied with heating rate as shown in Fig. 16. The decrease in ΔH for the second exothermic peak with decreasing the heating rate applied seems to indicate that the crystallization is proceeding gradually in the temperature range between the first and second exothermic peaks. At a heating rate of 10 K min^{-1}, the sum of ΔH for the first and second crystallization steps

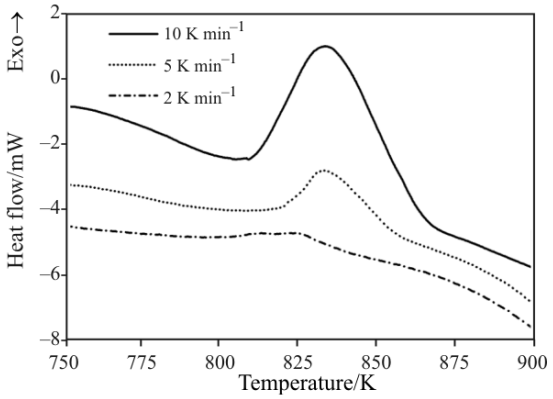

Fig. 15 Typical DSC curves for the second crystallization step of dehydrated ACC-ET at different heating rates

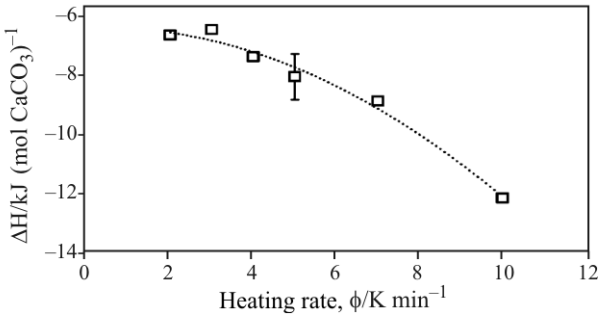

Fig. 16 Changes of ΔH value for the second crystallization step of dehydrated ACC-ET depending on heating rate applied

of dehydrated ACC-ET is about –31 kJ (mol $CaCO_3$)$^{-1}$, which is twice as large as that for the crystallization of dehydrated ACC-AQ.

Assuming a comparable thermodynamic state of the calcite phases crystallized from the dehydrated ACC-AQ and ACC-ET, it is expected that the amorphous phase of dehydrated ACC-ET is thermodynamically unstable with larger degree of atomic disordering compared with that of dehydrated ACC-AQ. Thus, number of the possible nucleation site and/or pre-existing nuclei seems to be very limited in the dehydrated ACC-ET. The linearly decreasing kinetic behavior observed for the first crystallization step of dehydrated ACC-ET is interpreted as the process controlled by the nucleation, which is characterized by the remarkable large value of E_a=304.1±23.6 kJ mol^{-1}. This indicates that the amorphous phase of dehydrated ACC-ET is preserved up to around 600 K by the higher kinetic barrier. Such amorphous formation processes through dehydration of precursor gel and stabilization mechanism of in situ produced amorphous material are similar to those of the glass formation by sol–gel method [67].

Conclusions

The amorphous calcium carbonates (ACC) prepared by two different methods in aqueous and ethanol media, i.e. ACC-AQ and ACC-ET, indicated the comparable IR spectra with that of the biogenic ACC. Both the samples were characterized as aggregates of nano-sized particles, where ACC-ET indicated a dried gel-like appearance. On heating the samples, thermal dehydrations took place in two steps, producing the dehydrated amorphous phases. The thermal dehydration process of ACC-ET was some more clearly separated in two steps as is observed for the biogenic ACC.

Large differences were observed between the thermally induced crystallization processes of the dehydrated ACCs to calcite. In agreement with the previous study, the dehydrated ACC-AQ was crystallized at around 600 K to calcite in a single step with ΔH= –13.1±0.2 kJ (mol $CaCO_3$)$^{-1}$. The three dimensional growth of pre-existing nuclei controlled by diffusion was proposed as an appropriate physico-geometric model of the crystallization process with the kinetic parameters E_a=270.7±15.1 kJ mol^{-1} and A=(9.19±0.03)·10^{22} s^{-1}. On the other hand, crystallization of the dehydrated ACC-ET proceeded through two steps in the largely separated temperature regions. The first step of crystallization took place with ΔH= –19.1±0.2 kJ (mol $CaCO_3$)$^{-1}$ at around 600 K as is the case of the dehydrated ACC-AQ. Although poorly crystalline phase of calcite with a small but detectable amount of vaterite phase was produced at this step, the surface texture of the sample did not change largely maintaining the dried gel-like appearance. The linearly decelerating rate behavior with E_a=379.8±26.0 kJ mol^{-1} and A=(9.40±0.03)·10^{32} s^{-1} of the first step of crystallization was interpreted as is controlled by nucleation process. At the second step of crystallization at around 825 K, the sample was transformed into fully crystalline calcite with a rightly stacking architecture.

The crystalline calcite phases obtained by heating ACC-AQ and ACC-ET decomposed quantitatively to CaO at the higher temperature than 900 K.

Acknowledgements

The present work is supported partially by a grant-in-aid for scientific research (B) (No. 18300267) from Japan Society for the Promotion of Science.

References

1 J. Johanson, H. M. Merwin and E. D. Williamson, Am. J. Sci., 33 (1916) 471.
2 G. Dorfmuler, Deut. Zuckerind., 63 (1938) 1217.
3 J. E. Gillott, J. Appl. Chem., 17 (1967) 18.
4 L. Brecevic and A. E. Nielsen, J. Cryst. Growth, 98 (1989) 504.
5 S. Raz, S. Weiner and L. Addadi, Adv. Mater., 12 (2000) 38.
6 I. M. Weiss, N. Tuross, L. Addadi and S. Weiner, J. Exp. Zool., 293 (2002) 478.
7 L. Addadi, S. Raz and S. Weiner, Adv. Mater., 15 (2003) 959.
8 S. Raz, P. C. Hamilton, F. H. Wilt, S. Weiner and L. Addadi, Adv. Funct. Mater., 13 (2003) 480.
9 Y. Politi, T. Arad, E. Klein, S. Weiner and L. Addadi, Science, 306 (2004) 1161.
10 S. Raz, O. Testeniere, A. Hecker, S. Weiner and G. Luquet, Biol. Bull., 203 (2002) 269.
11 Y. Levi-Kalisman, S. Raz, S. Weiner, L. Addadi and I. Sagi, Adv. Funct. Mater., 12 (2002) 43.

12 J. Aizenberg, G. Lambert, S. Weiner and L. Addadi, J. Am. Chem. Soc., 124 (2002) 32.
13 M. Li and S. Mann, Adv. Funct. Mater., 12 (2002) 773.
14 L. Xiang, Y. Xiang, Y. Wen and F. Wei, Mater. Lett., 58 (2004) 959.
15 M. Faatz, F. Grohn and G. Wegner, Adv. Mater., 16 (2004) 996.
16 C. Wang, J. Zhao, X. Zhao, H. Bala and Z. Wang, Powder Technol., 163 (2006) 134.
17 B. Guillemet, M. Faatz, F. Grohn, G. Wegner and Y. Gnanou, Langmuir, 22 (2006) 1875.
18 T. Kato, Adv. Mater., 12 (2000) 1543.
19 T. Kato, A. Sugawara and N. Hosoda, Adv. Mater., 14 (2002) 869.
20 K. Gorna, R. Munoz-Espi, F. Grohn and G. Wegner, Macromol. Biosci., 7 (2007)163.
21 L. B. Gower and D. J. Odom, J. Cryst. Growth, 210 (2000) 719.
22 X. Xu, J. T. Han and K. Cho, Chem. Mater., 16 (2004) 1740.
23 J. T. Han, X. Xu, D. H. Kim and K. Cho, Chem. Mater., 17 (2005) 136.
24 X. Xu, J. T. Han and K. Cho, Langmuir, 21 (2005) 4801.
25 X. Xu, J. T. Han, D. H. Kim and K. Cho, J. Phys. Chem. B, 110 (2006) 2764.
26 J. R. I. Lee, T. Y.-J. Han, T. M. Willey, D. Wang, R. W. Meulenberg, J. Nilsson, P. M. Dove, L. J. Terminello, T. van Buuren and J. J. D. Yoreo, J. Am. Chem. Soc., 129 (2007) 10370.
27 K. Sawada, Pure Appl. Chem, 69 (1997) 921.
28 L. Wang, I. Sondi and E. Matijevic, J. Colloid Interface Sci., 218 (1999) 545.
29 J. Aizenberg, A. J. Black and G. M. Whitesides, J. Am. Chem. Soc., 121 (1999) 4500.
30 W.-S. Kim, I. Hirasawa and W.-S. Kim, Ind. Eng. Chem. Res., 43 (2004) 2650.
31 K.-S. Seo, C. Han, J.-H. Wee, J.-K. Park and J.-W. Ahn, J. Cryst. Growth, 276 (2005) 680.
32 M. Faatz, F. Grohn and G. Wegner, Mater. Sci. Eng. C, 25 (2005) 153.
33 F. H. Wilt, Develop. Bio, 280 (2005) 15.
34 C. Gunther, A. Becker, G. Wolf and M. Epple, Z. Anorg. Allg. Chem., 631 (2005) 2830.
35 N. Koga, Y. Nakagoe and H. Tanaka, Thermochim. Acta, 318 (1998) 239.
36 S.-C. Huang, K. Naka and Y. Chujo, Langmuir, 23 (2007) 12086.
37 Y. Kojima, A. Kawanobe, T. Yasue and Y. Arai, J. Ceram. Soc. Jpn., 101 (1993) 1145, in Japanese.
38 H. S. Lee, T. H. Ha and K. Kim, Mater. Chem. Phys., 93 (2005) 376.
39 F. A. Andersen and L. Brecevic, Acta Chem. Scand., 45 (1991) 1018.
40 D. Chakrabarty and S. Mahapatra, J. Mater. Chem., 9 (1999) 2953.
41 J. W. McCauley and R. Roy, Am. Miner., 59 (1974) 947.
42 H. J. Meyer, Z. Kristallogr., 128 (1969) 183.
43 G. Wolf and G. Gunther, J. Therm. Anal. Cal., 65 (2001) 687.
44 H. L. Friedman, J. Polym. Sci. C, 6 (1964) 183.
45 T. Ozawa, Bull. Chem. Soc. Jpn., 38 (1965) 1881.
46 T. Ozawa, J. Thermal Anal., 2 (1970) 301.
47 T. Ozawa, Thermochim. Acta, 100 (1986) 109.
48 T. Ozawa, J. Thermal Anal., 31 (1986) 547.
49 N. Koga, Thermochim. Acta, 258 (1995) 145.
50 M. E. Brown, D. Dollimore and A. K. Galwey, Reactions in the Solid-State, Elsevier, Amsterdam 1980.
51 J. Šesták, Thermophysical Properties of Solids, Elsevier, Amsterdam 1984.
52 A. K. Galwey and M. E. Brown, Thermal Decomposition of Ionic Solids, Elsevier, Amsterdam 1999.
53 J. Šesták, Science of Heat and Thermophysical Studies, Elsevier, Amsterdam 2005.
54 J. Šesták, J. Thermal Anal., 33 (1988) 1263.
55 N. Koga, J. Malek, J. Šesták and H. Tanaka, Netsu Sokutei, 20 (1993) 210.
56 R. Ozao and M. Ochiai, J. Ceram. Soc. Jpn., 101 (1993) 263.
57 N. Koga and H. Tanaka, J. Thermal Anal., 41 (1994) 455.
58 N. Koga and H. Tanaka, Thermochim. Acta, 388 (2002) 41.
59 J. Šesták and G. Berggren, Thermochim. Acta, 3 (1971) 1.
60 D. M. Bates and D. G. Watts, Nonlinear Regression and its Applications, Wiley, New York 1988.
61 N. Koga, A. Mako, T. Kimizu and Y. Tanaka, Thermochim. Acta, 467 (2008) 11.
62 L. A. Perez-Maqueda, J. M. Criado and P. E. Sanchez-Jimenez, J. Phys. Chem. A, 110 (2006) 12456.
63 N. Koga, Thermochim. Acta, 244 (1994) 1.
64 A. K. Galwey and M. Mortimer, Int. J. Chem. Kinet., 38 (2006) 464.
65 P. Budrugeac, V. Musat and E. Segal, J. Therm. Anal. Cal., 88 (2007) 699.
66 J. M. Criado, P. E. Sanchez-Jimenez and L. A. Perez-Maqueda, J. Therm. Anal. Cal., 92 (2008) 199.
67 S. Sakka, J. Sol-Gel Sci. Technol., 3 (1994) 69.

DOI: 10.1007/s10973-008-9110-3